Mapping the annual dynamics of cultivated land in typical area of the Middle-lower Yangtze Plain using Long Time-series of Landsat Images based on Google Earth Engine

Yuhao Jin[a,b],Xiaoping Liu[a,b*],Jing Yao[c] , Xiaoxiang Zhang[d] , Han Zhang[a,b]

[a]School of Geography and Planning, Sun Yat-sen University, Guangzhou 510275, China;[b]Guangdong Key Laboratory for Urbanization and Geo-Simulation, Sun Yat-sen University, Guangzhou 510275, China;[c]Urban Big Data Centre,School of Social and Political Science, University of Glasgow,Glasgow G12 8RZ,UK;[d]School of Earth Sciences and Enginneering,Hohai University, Nanjing 211100,China

Cultivated land in Middle-lower Yangtze Plain has been greatly reduced over the last few decades due to rapid urban expansion and massive urban construction. Accurate and timely monitoring of cultivated land changes has significant for regional food security and the impact of national land policy on cultivated land dynamics. However, generating high-resolution spatial-temporal records of cultivated land dynamics in complex areas remains difficult due to the limitations of computing resources and the diversity of land cover over a complex region. In our study, the annual dynamics of cultivated land in Middle-lower Yangtze Plain were first produced at 30 m resolution with a one-year interval in 1990-2010.Changes of vegetation and cultivated land are examined with the breakpoints inter-annual Normalized Difference Vegetation Index (NDVI) trajectories and synthetic NDVI derived by the enhanced spatial and temporal adaptive reflectance fusion model (ESTRAFM), respectively. Last, cultivated land dynamics is extracted with a one-year interval by detecting phenological characteristic. The results indicate that the rate of reduction in cultivated land area has accelerated over the past two decades, and has intensified since 1997.The dynamics of cultivated land mainly occurred in the mountains, hills, lakes and around towns, and the change frequency of these area was mainly one or two times. In particular, the changes in cultivated land in Nanjing have been most intense, perhaps attributed to urban greening and infrastructure construction.

Keywords: Cultivated land, change detection, NDVI trajectory, Google Earth Engine, ESTARFM

1. Introduction

Cultivated land dynamics have manifold effects on both ecosystems and human society (Foley et al. 2011). They are particularly crucial to food security and overall sustainable development in China, a large country of more than 1.3 billion people. The changes in cultivated land in the Middle-lower Yangtze plain, the most developed region in the country, represents a microcosm of the dynamics of cultivated land in China. With the acceleration of urbanization and industrialization in the past two

decades, the conflict between the supply and demand of cultivated land in the Middle-lower Yangtze plain has become more intense. Effective monitoring of cultivated land dynamics has important policy implications for the management of food security and the improvement of rural livelihoods (Yu et al. 2013; Estel et al. 2015).According to China's National Land Resources Survey data, the area of cultivated land has changed dramatically in recent decades, but detailed information about the spatial distribution of cultivated land has not been provided to the scientific community. In fact, China's cultivated land inventory data will take several years to complete and cannot provide information on continuous changes in cultivated land every year, especially in complex farming regions (Liu, Kuang, Zhang, Xu, Qin, Ning, Zhou, Zhang, Li, Yan, et al. 2014). However, the annual change in cultivated land is important information for the study of cultivated land protection, food security and ecological environments. It is urgent that the public and the scientific community map spatial distribution of the annual dynamics of cultivated land at a high spatiotemporal resolution.

Remote sensing (RS), because it can over a long time span and is low cost, has been a popular technique to detect land use/cover change (LUCC) (Liang et al. 2018; Liu et al. 2017; Liu et al. 2018). Many RS data products have been product for cultivated land dynamics in China (Jin et al. 2018). For example, China's Land-Use/Cover Datasets were created by visual interpretation of RS images for every five years between 1980 and 2015 (Liu, Kuang, Zhang, Xu, Qin, Ning, Zhou, Zhang, Li, Yan, et al. 2014).However, these products mainly focused on the use of two or more Landsat images with intervals of five or ten years, ignoring the changes in cultivated land at finer temporal scales (Graesser et al. 2015; Xiong et al. 2017). Although long time-series of RS data have been used for various applications, it is time and resource intensive to process and analyze these data. Since Google launched Earth Engine (GEE) in 2010, which can quickly process large amounts of RS images, a number of studies have attempted to use long time series of RS images to detect LUCC, such as changes to forest and water resources (Xiong et al. 2017).Given the complexity and high computational costs of RS image processing, GEE provides a new platform and opportunities for detecting LUCC at finer spatial and temporal scales.

Not only Modis images but also Landsat images have been used to detect changes in cultivated land, such as identifying the abandonment of cultivated land in Northern Kazakhstan (Beurs, Henebry, and Gitelson 2004) and abandoned farmland in the Central Plains of the United States (Wardlow and Egbert 2008).The latter was used to study abandoned farmland in Central and Eastern Europe (Camilo et al. 2013) and to identify the farmland dynamics in Europe during 2001 to 2012 (Estel et al. 2015).

However, due to the influence of the subtropical monsoon and typhoon in the southeast coast of China, it is difficult to derive information about cultivated land from single-source RS images. Thus, spatiotemporal fusion is often employed to integrate multi-source images to obtain high spatial-temporal land use/cover data (Hilker et al. 2009). In particular, the Spatial and Temporal Adaptive Reflectance Fusion Model (STARFM) estimates fine resolution images based on the spatial and spectral weighted differences between pairs of fine and rough spatial resolution images and the coarse spatial resolution images collected on the prediction day (Feng et al. 2006).An enhanced STARFM (ESTARFM) was further proposed to improve the applicability of STARFM to spatially heterogeneity regions (Zhu et al. 2010). This paper attempts to utilize ESTRAFM to generate synthetic Normalized Difference Vegetation Index (NDVI) at high spatial and temporal resolution to extract information about cultivated land.

The goal of this research is to identify a method for detecting cultivated land dynamics using long time-series trajectory methods. First, we detect changes in vegetation dynamics using the breakpoints

by multi-year NDVI time series. Then, we generate synthetic Landsat NDVI time series at 30-m spatial resolution and 15-day temporal resolution to extract phenological features for cultivated land change detection. Last, we also assess the temporal and spatial differences in cultivated land dynamics in the Middle-lower Yangtze Plain over the past two decades (1990-2010).

2. Study Area and Data

2.1 Study area

The Middle-lower Yangtze Plain is a densely populated area in China with a well-developed economy and culture. The cultivated land is dominated by red soil, which mainly supports crops ~~of~~such as paddy rice, rape, vegetables and wheat, according to the China Statistical Yearbook for Regional Economy (Guo 2014). In spring, the middle season rice, late rice or maize are planted in April, and they are collected in September. In contrast, wheat or rape are planted in September and are collected in the next March. With the development of social economy and productivity in recent decades, the conversion of cultivated land to urban construction has put great pressure on the sustainability of urban development. The study area is located along the Yangtze River Plain at the border of the Jiangsu and Anhui Provinces, covering an area of 10058.2 km² (Figure 1). As a famous paddy rice region, the study area has many rural settlements and is an important base of production of grain and oil in China.

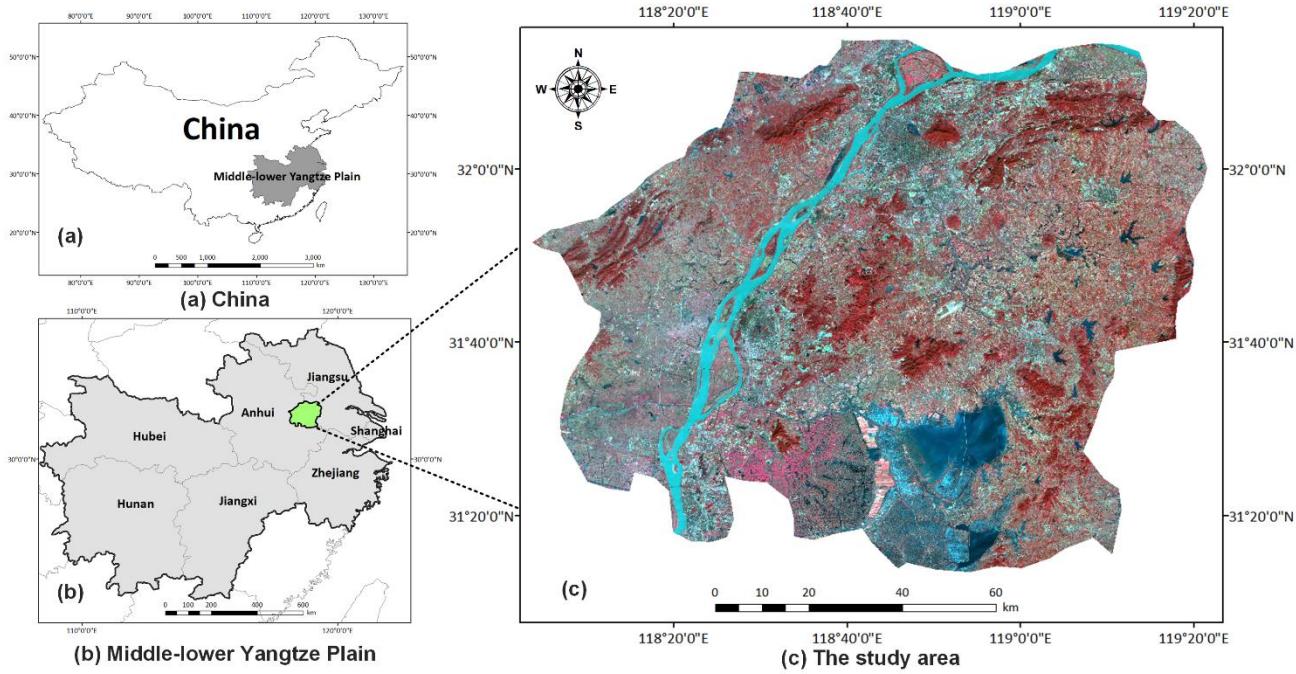

Figure 1. Study area in the border area of Jiangsu province and Anhui Province. The study area displays the red, near infrared band and middle infrared band of the Landsat Thematic Mapper (TM) data with blue, green, and red color.

2.2 Satellite data on Google Earth Engine

GEE has made it possible for the first time in history to rapidly and accurately process vast amounts of satellite imagery, identifying where and when land cover change has occurred at high resolution (Gorelick et al. 2017). Decades of historical images and scientific datasets are stored in GEE (Yu and Gong 2012). Most Landsat data can be accessed and downloaded online through the GEE platform, which includes Landsat 5 TM, Landsat 7 ETM+ and Landsat 8 OLI/TIRS (Patel et al. 2015). In this study, we used all the available atmospherically corrected surface reflectance images from Landsat 5 from 1990 to 2010. These data have been atmospherically corrected using LEDAPS, which is generated by Google and supplied by USGS.

3. Methods

Several techniques were employed in this research to explore the cultivated land dynamics. First, NDVI was calculated for all of the Landsat images, from which the annual and monthly NDVI composites were derived. Then, vegetation dynamic change were identified using the breakpoints and the time periods from the annual long time-series NDVI trajectory. Then, the ESTRAFM (Enhanced Spatial and Temporal Adaptive Reflectance Fusion Model) approach was used to generate the synthetic NDVI with 30-m spatial resolution and 15-day temporal resolution. Finally, based on the vegetation dynamics and the synthetic Landsat NDVI time-series data, cultivated land changes were investigated using phenological characteristics.

3.1 Pre-processing of Landsat images

In our study, the Landsat footprint path 120/row 038, World Reference System (WRS)-2, were used to map the cultivated land dynamics. These images contain 4 visible and near-infrared (VNIR) bands and 2 short-wave infrared (SWIR) bands processed to orthorectified surface reflectance, and one thermal infrared (TIR) band processed to orthorectified brightness temperature. The visble, VNIR and SWIR bands have a resolution of 30m / pixel. The TIR band, while originally collected with a resolution of 120m / pixel has been resampled using cubic convolution to 30m by Google Earth Engine.

As clouds might cause missing values or outliers in the long time-series of Landsat data and could affect the calculation of NDVI, a built-in function from GEE was used to remove the effect of cloud from the Landsat images. This function is a rudimentary cloud scoring algorithm that ranks Landsat pixels by their relative cloudiness. Temperature, brightness and the combined Normalized Difference Snow Index are used to calculate a simple cloud score ranging from 0 to 100 and remote sensing images with a cloud score greater than 20 are masked.

3.2 Inter-annual NDVI trajectory

The NDVI was calculated from the time series of Landsat Surface Reflectance image collection using equation (1), which reflects the optical difference in the vegetation between the visible and the

near infrared bands and the soil background. The NDVI values vary between -1 and 1 for different land cover types.

$$\mathrm{NDVI} = (R_{\mathrm{nir}} - R_{\mathrm{r}}) / (R_{\mathrm{nir}} + R_{\mathrm{r}}) \quad (1)$$

where R_{nir} is the calibrated top-of-atmosphere reflectance of the near-infrared band, R_r is the calibrated top-of-atmosphere reflectance of the red band.

The maximum and minimum normalized difference vegetation indexes (NDVIs) describe three extremes of vegetation greenness during a predefined period. For example, the maximum annual composite NDVI represents the greenest status of vegetation during the entire year, which can differentiate the vegetated surface from the nonvegetated surface (Jamali et al. 2014). Similarly, the minimum annual composite NDVI represents the least greenness status of vegetation, which is the vegetation growth baseline for extracting the phenology (White, Thornton, and Running 1997).Therefore, two composites of NDVI value were created: the composite of the minimum and the maximum NDVI per year, and the mean NDVI per year, which can be exported form GEE after the calculation of required NDVI values.

A method detecting vegetation dynamics by breakpoints in multi-year NDVI profiles was ~~generated~~ used to detect the spatial distribution of non-vegetation, vegetation increase, vegetation decrease and continuous vegetation (Schmidt et al. 2015). Therefore, the breakpoints at which the major changes occurred within a certain period can be detected (Huang et al. 2017).

First, the land cover was considered non-vegetation if the entire maximum NDVI value of the minimum inter-annual NDVI was less than a defined threshold (0.2 in this study). There was also an obvious difference between the maximum NDVI trajectory of non-vegetation and vegetation, for example, among residential land, waterbody and vegetation. Second, as seen in Figure 2, the mean NDVI value was used to identify three categories including a 'NDVI increase', a 'NDVI decrease' and a 'No NDVI change'. Thresholds of 0.25, 50% and 50% were employed for the threshold and percentage of NDVI phase change and the percentage of NDVI phase changes over the entire time series, respectively, which conformed to the general rule of vegetation increase or decrease. In addition, 'no NDVI change' cannot be defined as vegetation increase or vegetation decrease when the NDVI was not changed or when the change was too small. That is, the three categories, 'NDVI increase', 'NDVI decrease' and 'No NDVI change' corresponded with 'vegetation increase', 'vegetation decrease 'and 'continuous vegetation'.

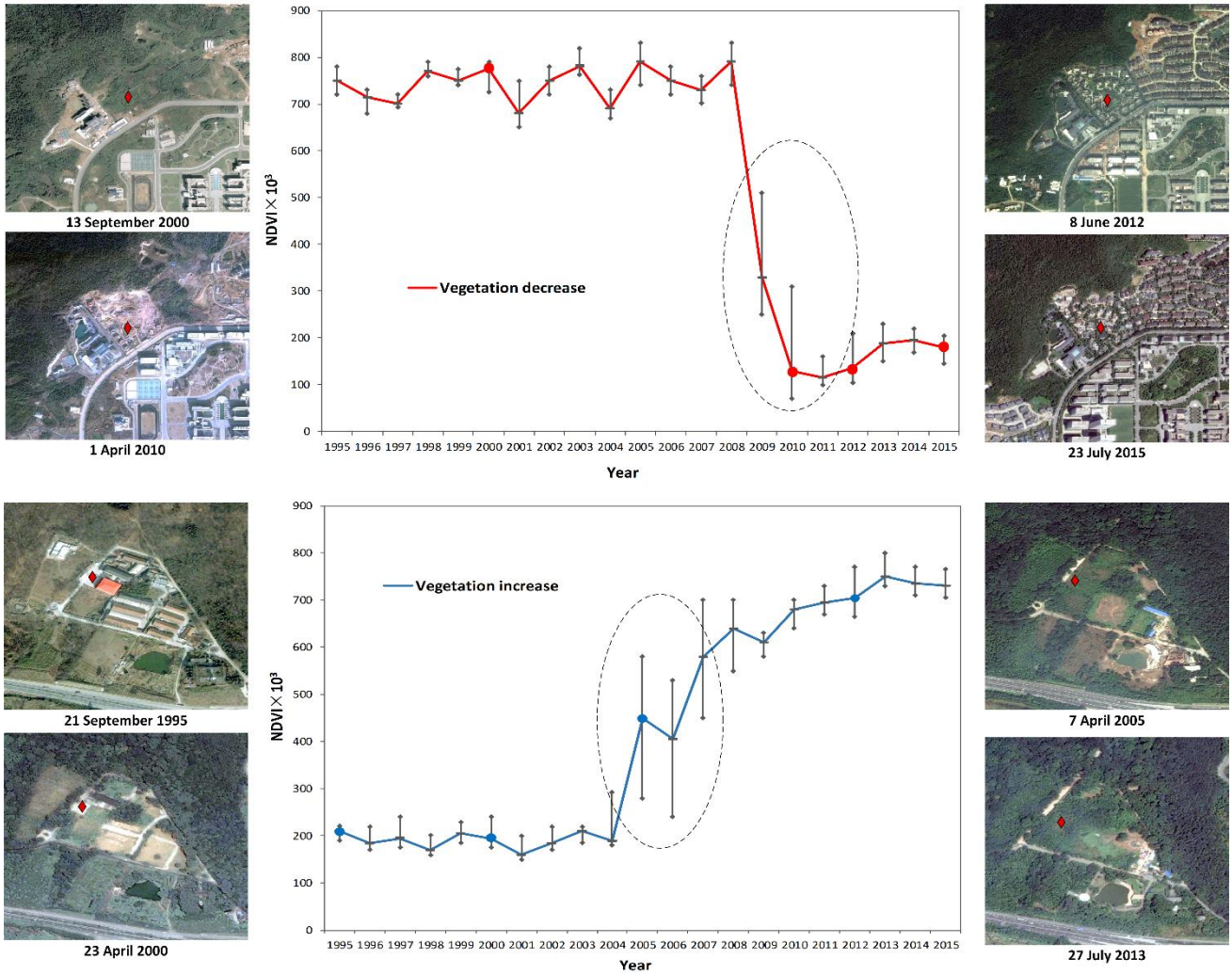

Figure 2. Changes in inter-annual time series NDVI trajectories when vegetation is decreased (red line) or vegetation is increased (blue line). Example of a temporal segmentation with Google Earth images (RGB: Red, Green, Blue), for pixels represented by red diamond symbols. The red and blue dots on the NDVI trajectories represent the Google Earth Images of the corresponding year.

To verify the accuracy of the detection of vegetation loss and gain, visual interpretation of 2000 samples (100 per year) of all images involved was implemented, which were stratified according to four types (non-vegetation, vegetation increase, vegetation decrease and continuous vegetation). The sample size corresponds to the spatial resolution of remotely sensed data (Basnet and Vodacek 2015). One sample means one pixel which represents the size of a pixel in Landsat Thematic Mapper (TM) data. These samples came from the visual interpretation of selected satellite images by the experienced mappers. Meanwhile, high spatial resolution Google Earth images and China's Land-Use/cover Datasets (CLUDs) provided significant references for the visual interpretation (Liu, Kuang, Zhang, Xu, Qin, Ning, Zhou, Zhang, Li, and Yan 2014).

3.3 Spatiotemporal fusion for synthetic NDVI time series

As the Landsat images with few clouds in the study area were not sufficient to generate 15-day temporal resolution time series of NDVI, a spatiotemporal fusion algorithm, ESTARFM, was employed to integrate the information from Landsat and MODIS or AVHRR images. ESTARFM was an effective and efficient approach for generating high spatial-temporal resolution NDVI in a complex area, and was suitable for this study area (Zhu et al. 2010).

ESTARFM utilizes two pairs of coarse resolution and fine resolution remote sensing images with similar dates at the base date t_m as well as t_n. If the fine resolution and the corresponding coarse resolution reflectance are obtained at t_0 and another coarse resolution is obtained at t_p, the fine resolution reflectance of the base date t_p can be calculated as follows:

$$F(x, y, t_p) = F(x, y, t_0) + c(x, y) \times (H(x, y, t_p) - H(x, y, t_0)) \quad (2)$$

Formula 3 indicates the relationship between the fine resolution reflectance F(x,y) and the coarse resolution reflectance H(x,y) from different dates t_p and t_0. The internal conversion coefficient c(x,y) can be obtained by linear regression of the fine-resolution and coarse resolution reflectance at t_m and t_n.

At the same time, ESTARFM uses the moving window to use information from similar pixels and integrate them into the fine resolution reflectivity calculation, as follows:

$$F(x_{z/2}, y_{z/2}, t_p) = F(x_{z/2}, y_{z/2}, t_0) + \sum_{i=1}^{N} Zi \times Ci \times (H(x_i, y_i, t_p) - H(x_i, y_i, t_0)) \quad (3)$$

where (x_i,y_i) is the coordinates of the i th similar neighboring pixel, and Z_i is the weight of the i th similar pixel, assuming z is the search window size, where a similar pixel is defined as a pixel with a close surface reflectance in the window.

In addition, the temporal weights W_m and W_n are calculated using the change in the coarse resolution reflectance between the different dates t_m, t_n and the predictive date t_p, as expressed in (4) and (5).

$$W_m = \frac{1/\left|\sum_{j=1}^{z}\sum_{l=1}^{z} H(x_j, y_l, t_m) - \sum_{j=1}^{z}\sum_{l=1}^{z} H(x_j, y_l, t_p)\right|}{\sum_m (1/\left|\sum_{j=1}^{z}\sum_{l=1}^{z} H(x_j, y_l, t_m) - \sum_{j=1}^{z}\sum_{l=1}^{z} H(x_j, y_l, t_p)\right|)} \quad (4)$$

$$W_n = \frac{1/\left|\sum_{j=1}^{z}\sum_{l=1}^{z} H(x_j, y_l, t_n) - \sum_{j=1}^{z}\sum_{l=1}^{z} H(x_j, y_l, t_p)\right|}{\sum_n (1/\left|\sum_{j=1}^{z}\sum_{l=1}^{z} H(x_j, y_l, t_n) - \sum_{j=1}^{z}\sum_{l=1}^{z} H(x_j, y_l, t_p)\right|)} \quad (5)$$

By combining the fine resolution reflectance with the temporal weights W_m and W_n, the final fine resolution reflectance at the predictive date t_p is obtained, as follows:

$$F(x_{z/2}, y_{z/2}, t_p) = W_m \times F_m(x_{z/2}, y_{z/2}, t_m) + W_n \times F_n(x_{z/2}, y_{z/2}, t_n) \quad (6)$$

ESTARFM utilizes two pairs of coarse resolution and fine resolution remote sensing images with similar dates. For example, two pairs of Landsat TM and MODIS images were used to predict the image at the Landsat spatial resolution at the predictive date. Thus, the synthetic NDVI images have the same spatial resolution as the Landsat images. In addition, to investigate crucial months and phenological stages in the detection of cultivated land dynamics, the monthly NDVI trajectory of cultivated land was generated from the synthetic NDVI images. As the input of the spatiotemporal fusion model, Landsat and MODIS images are selected based on the minimum cloud amount (Figure 3).

Table 1. The number of used and simulated images

Year	The number of Landsat images used	The number of ESTARFM-based synthetic images	Year	The number of Landsat images used	The number of ESTARFM-based synthetic images
1990	6	18	2001	6	18
1991	7	17	2002	7	17
1992	8	16	2003	6	18
1993	5	19	2004	6	18
1994	8	16	2005	5	19
1995	5	19	2006	6	18
1996	6	18	2007	5	19
1997	6	18	2008	5	19
1998	8	16	2009	9	15
1999	8	16	2010	8	16
2000	7	17			

3.4 Mapping cultivated land dynamics

In this study, the synthetic high spatial-temporal resolution NDVI trajectories were used to distinguish between cultivated and non-cultivated land using vegetation cover indicated by phenological characteristics. Given the high fit and accuracy of the Savitzky-Golay filtering method, the S-G filter was used to process the monthly Landsat NDVI time-series composites to minimize the influence of noise , as shown in (7) where Y^* is the filtered NDVI value and Y is the original NDVI value (Savitzky and Golay 1964). Ci is the coefficient of the Savitzky-Golay filter, and the coefficient j is the coefficient of the original NDVI data table.

$$Y_j^* = (2m+1)^{-1} \sum_{i=-m}^{i=m} C_i Y_{j+1} \quad (7)$$

The rules for using crop phenological feature extraction to distinguish between cultivated land and vegetative-land in our study are based on the Growth Period Data of Major Crops in China, with support from the Compilation of Digital Atlas of Agricultural Climate Resources in China (Grant No.2007FY120100) and National Science & Technology Infrastructure of China (Table 2).

Table 2. Features for cultivated land extraction.

Feature	Description	Rules
Row	NDVI value for winter wheat reviving	Landsat NDVI value DOY:050-070
How	NDVI value for winter wheat heading	Landsat NDVI value DOY:110-130
Pow	NDVI value for winter wheat ripening	Landsat NDVI value DOY:150-170
Tor	NDVI value for rice transplanting	Landsat NDVI value DOY:180-200
Hor	NDVI value for rice heading	Landsat NDVI value DOY:210-230
Ror	NDVI value for rice ripening	Landsat NDVI value DOY:270-290
Roo	NDVI value for oilseed rape reviving	Landsat NDVI value DOY:050-070
Hoo	NDVI value for oilseed rape heading	Landsat NDVI value DOY:110-130
Poo	NDVI value for oilseed rape ripening	Landsat NDVI value DOY:150-170
Som	NDVI value for maize sowing	Landsat NDVI value DOY:170-190
Hom	NDVI value for maize heading	Landsat NDVI value DOY:200-220
Rom	NDVI value for maize ripening	Landsat NDVI value DOY:260-280

Twelve phenological features of crops were extracted from the synthetic NDVI time series to separate cultivated land dynamics from non-cultivated land dynamics, including the winter wheat reviving (Row), winter wheat heading (How), winter wheat ripening (Pow), rice transplanting (Tor), rice heading (Hor), rice ripening (Ror) , oilseed rape reviving (Roo), oilseed rape heading (Hoo), oilseed rape ripening (Poo), maize sowing (Som), maize heading (Hom), maize ripening (Rom).

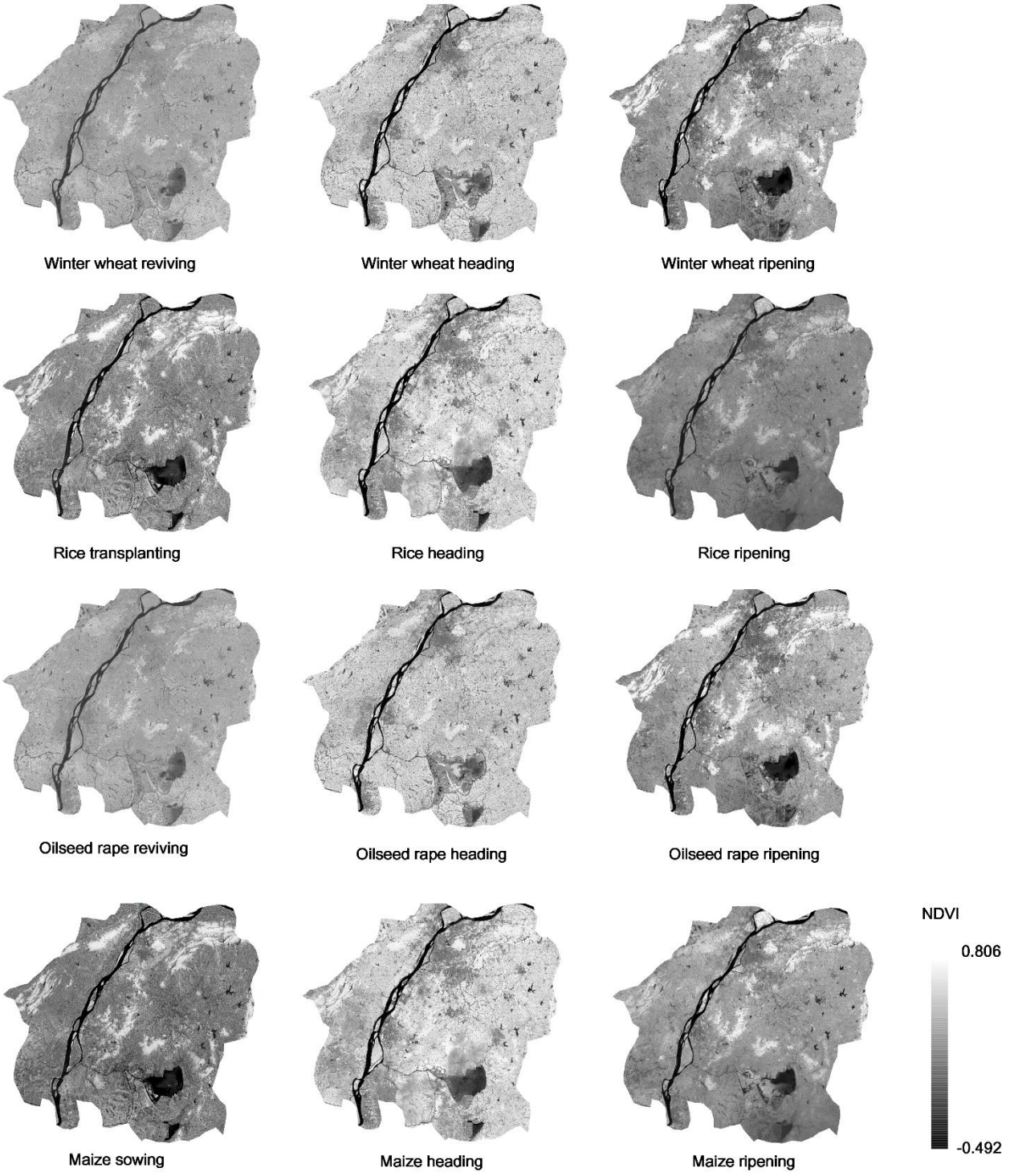

Figure 3.Twelve phenological features extracted from the synthetic NDVI time series

Based on the China Agrometeorological Station in Gaochun (118°52′,31°19′) (http://data.cma.cn/site/index.html), the NDVI time series of cultivated land at Gaochun Agrometeorological Station was used to determine the threshold setting of cultivated land in this area. Twelve phenological features of crops at agrometeorological stations were extracted as references to distinguish the range in the threshold of change in the cultivated land dynamics in the study area.

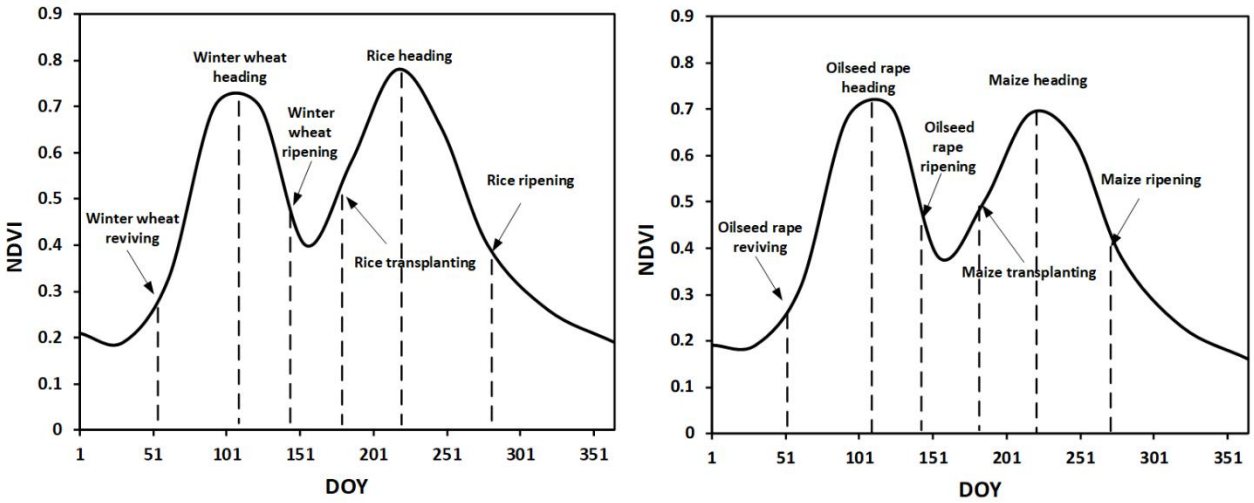

Figure 4. The crop growth curve of cultivated land in the study area

As shown in Figure 3, the NDVI time series of cultivated land at the Agrometeorological Station shows they practice one cropping of winter wheat per spring and one cropping of rice per autumn, which represents the multiple cropping of winter wheat and rice. First, Row and Pow should be less than given thresholds (0.3, 0.5 in this study) and How should be greater than 0.6, which is consistent with the phenological features of winter wheat. Then, Tor and Ror should be less than the given thresholds (0.5, 0.4 in this study) and Hor should be greater than 0.6, which is consistent with the phenological features of rice. Meanwhile, in order to consider the types of maize and rape in the study area, Roo and Poo should be less than given thresholds (0.3, 0.45 in this study) and How should be greater than 0.65. Besides, Som and Rom should be less than the given thresholds (0.5, 0.4 in this study) and Hom should be greater than 0.55. To highlights the phenological features of cultivated land dominated by soil and having no crops were planted in the study area, the minimum value of monthly NDVI should be less than a given threshold (0.2 in this study). We found that the NDVI time series of cultivated land and non-cultivated land are quite different in the study area.

Three parameters were used to define different phases of cultivated land changes, including vegetation change (Vc), the land cover class in the year prior to the change (Pre) and the land cover class in the year following the change (Lat). Table 3 shows the rules for determining the phases of cultivated land changes, which includes vegetation increase (Vi),vegetation decrease (Vd),Continuous vegetation (Cv),Cultivated land (Cl),Non-cultivated land (Ncl).For example, the increase is converted from residential land or water bodies to cultivated land, if the landcover class of the latter year is cultivated land in the area of vegetation increase; the increase was converted from grassland or forest to cultivated land, if landcover class of the previous year is non-cultivated land and the class of the latter year is cultivated land in the area of continuous vegetation. In contrast, if the landcover class of the previous year is cultivated land in the vegetation decrease area, the decrease was converted from cultivated land to residential land or water bodies; if the landcover class of the previous year is cultivated land and the class of the latter year is non-cultivated land in the area of continuous vegetation, the decrease was converted from cultivated land to grassland or forest. In addition,other areas that did not meet the above requirements are the areas represent areas without cultivated land changes.

Table 3. Classification rules of cultivated land dynamic change based on vegetation change detection categories

Class	Dynamics	Rules
Cultivated land increase	Residential land or waterbody to cultivated land	Vc = Vi and Lat = Cl
	Grassland or forest to cultivated land	Vc = Cv and Pre = Ncl and Lat = Cl
Cultivated land decrease	Cultivated land to residential land or waterbody	Vc = Vd and Pre = Cl
	Cultivated land to grassland or forest	Vc = Cv and Pre = Cl and Lat = Ncl
Continuous Cultivated land	Cultivated land to Cultivated land	Vc = Cv and Pre = Cl and Lat = Cl
Non-cultivated land	Non-cultivated land to Non-cultivated land	Other areas that do not meet the requirements of ultivated land increase,cultivated land decrease and continuous cultivated land

The frequency of cultivated land change per pixel was calculated by counting how often a pixel was identified as cultivated land increase or decrease for twenty years. The recorded frequency of change is 0 if the same pixel in the next two years is cultivated land or non-cultivated land, indicating that the category of the pixel has not changed.

4 Results

4.1 Vegetation dynamics

To map the dynamic change in cultivated land in the Middle-lower Yangtze Plain, we first extract increase and decrease in vegetation from the time series inter-annual NDVI and detect the change in vegetation dynamic in the Middle-lower Yangtze Plain for the 1990-2010 period. Figure 5 shows the distribution of four types of changes in vegetation including vegetation decrease, vegetation increase, continuous vegetation and non-vegetation. Over the past twenty years, the area and frequency of vegetation decrease were greater than that of vegetation increase. It can be observed that vegetation decreased relatively slowly before 2000, and the decrease in vegetation obviously accelerated in the 1st decade of the 21st century.

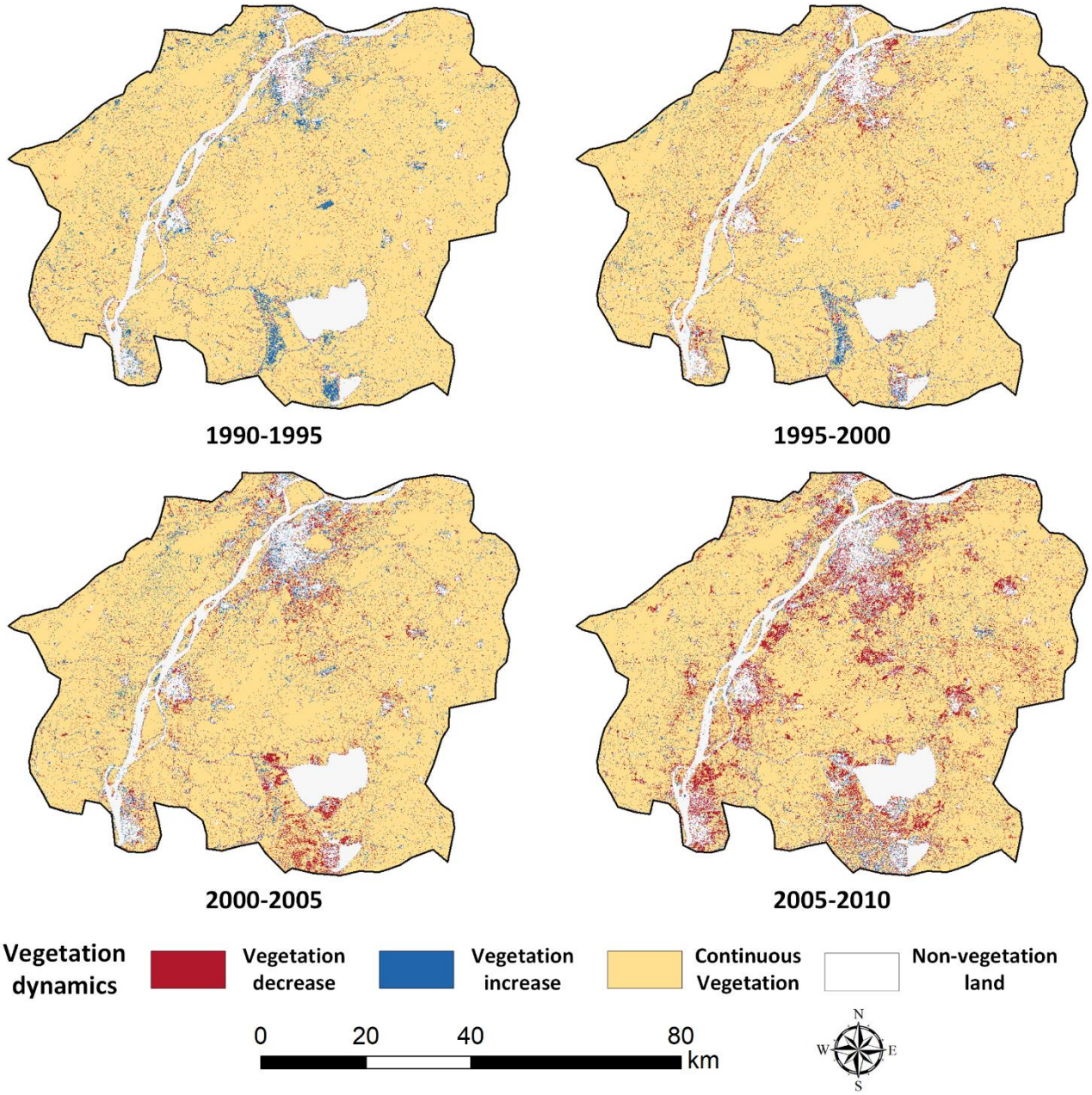

Figure 5. The study area with vegetation decrease and vegetation increase from 1990 to 2010.

4.2 Cultivated land increase and decrease

We synthesized the high spatial-temporal resolution NDVI time series using the ESTARFM model to obtain the NDVI trajectory, which can differentiate cultivated land from vegetation, since we found that the original Landsat monthly NDVI time in the study area was insufficient to characterize the process of vegetation growth. Based on synthetic high spatial-temporal resolution Landsat NDVI time-series data, we separated cultivated land dynamics from non-cultivated land dynamics by detecting phenological changes and the sequential temporal information of vegetation growth.

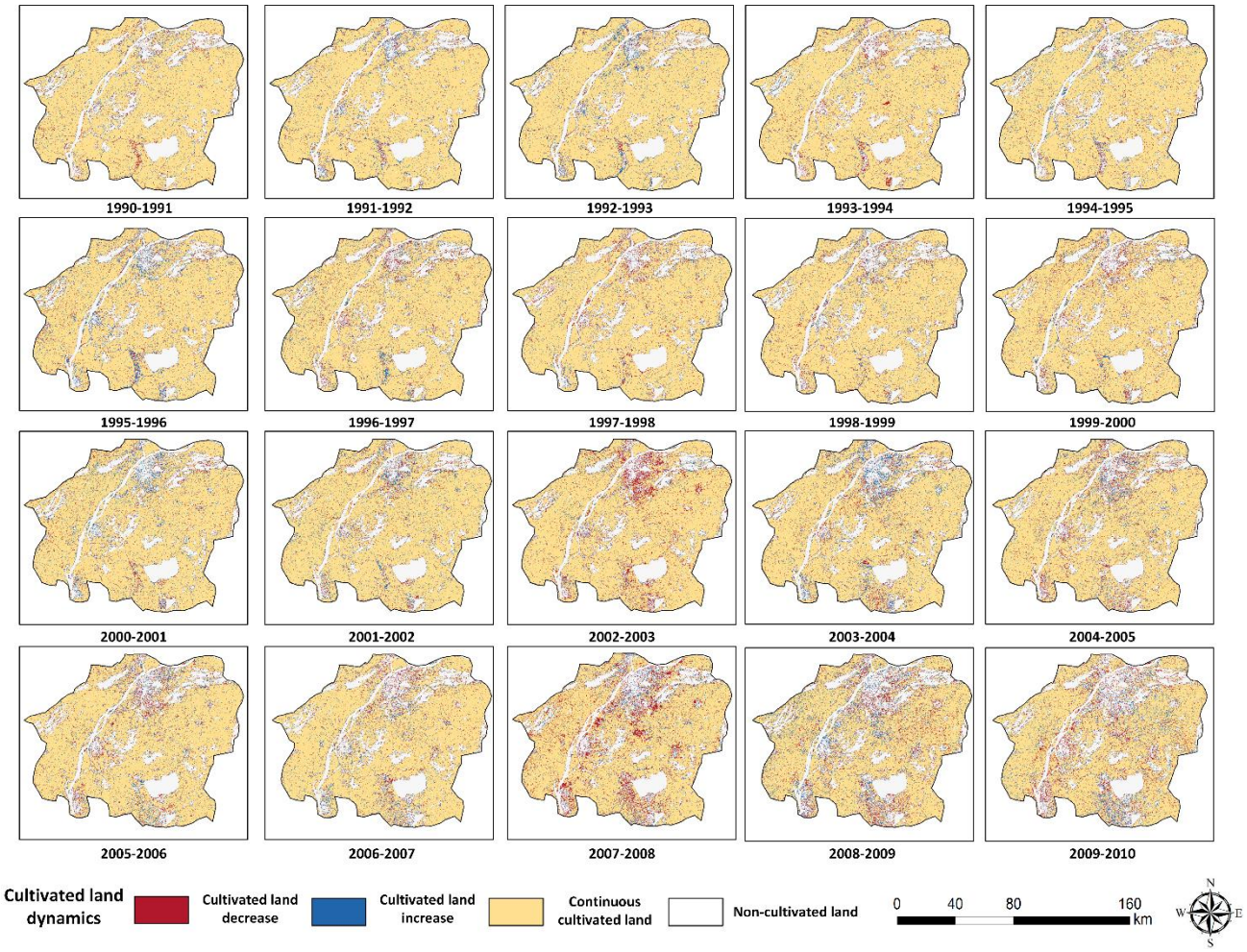

Figure 6. Cultivated land dynamics of Middle-lower Yangtze Plain in past two decades (1990-2010)

Figure 6 shows the distribution of the final four types cultivated land change (cultivated land decrease, cultivated land increase, continuous cultivated land and non-cultivated land). The total area of cultivated land decreased from 1990 to 2010. Although the total area of cultivated land was reduced, the increase in cultivated land and the decrease in cultivated land in different years were also different. The rate of cultivated land area reduction in the last two decades has gradually become faster and the decrease in cultivated land has become more intense since 1997. Cultivated land decreased by more than 260 km^2 annually from 2002 to 2010, with the largest reduction of 295 km^2 in 2007-2008. In contrast, 2005-2006 was the year with the most cultivated land increased, during which cultivated land increased by 227 km^2,-and the year with the smallest increase of cultivated land was 1999-2000, during which cultivated land increased by 175 km^2 (Table 4).

Table 4. The time series of areas of the cultivated land dynamics categories

Year	Cultivated land decrease (km^2)	Cultivated land increase (km^2)	Continuous cultivated land (km^2)	Non-cultivated land (km^2)
1990-1991	188	183	6869	2818
1991-1992	194	192	6848	2824
1992-1993	201	197	6824	2836
1993-1994	191	178	6818	2871
1994-1995	200	193	6783	2882
1995-1996	213	205	6740	2900
1996-1997	221	214	6695	2928
1997-1998	227	196	6653	2982
1998-1999	226	190	6596	3046
1999-2000	224	175	6519	3140
2000-2001	220	188	6413	3237
2001-2002	234	195	6271	3358
2002-2003	267	214	6190	3387
2003-2004	269	202	6079	3508
2004-2005	262	192	5950	3654
2005-2006	280	227	5841	3710
2006-2007	272	221	5744	3821
2007-2008	295	196	5606	3961
2008-2009	289	213	5430	4126
2009-2010	292	201	5240	4325

Figure 6 further indicates that the cultivated land decreased slowly from 1990 to 1997, during which time 1408 km^2 of land was underwent cultivated land decrease and 1362 km^2 was revegetated. After that, the rate of reduction in cultivated land accelerated from 1997 to 2002. The net decrease in the area of cultivated land was 187 km^2, which was nearly four times that of the previous stage.

Next, we found that the cultivated land area began to decline rapidly from 2002 to 2007 with an obvious cultivated land decrease in 2002-2003.The total area of cultivated land decreased by 1350 km^2 in 5 years and the net decrease in cultivated land area was 324 km^2, which implied an average decrease of 294 km^2 per year and average net decrease of 59 km^2. According to Jiangsu Statistical Yearbook 2002 – 2007, the total population of the study area increased from 7.99 million in 2002 to 8.83 million in 2007, with an increase of 840 thousand people. Meanwhile, the GDP of the study area has increased by about 2.5 times in the five years, which changed from 182.1 billion yuan in 2002 to 459.6 billion yuan in 2007. It can be figured out that urban land expansion brought about by economic and population growth may be the most important and fundamental driving factor leading to the rapid reduction of cultivated land in this stage. What's more, Nanjing made a major administrative adjustment in 2002, which pointed out that the urban area of Nanjing should be expanded from 1026.21 square kilometers in 2002 to 4723.07 square kilometers. In 2002, Nanjing urban planning also put forward the idea of "taking the Yangtze River as the main axis, taking the main city as the core, with multiple structures, spacing distribution, multi-center and open spatial pattern of urban development zones"(Mei et al. 2010). This indicates that the land use structure of Nanjing has begun to change greatly.

Then, after 2007, the cultivated land in the study area continued to decrease and the rate of cultivated land reduction has further accelerated, with an obvious cultivated land decrease in 2007-2008. The net

decrease in the area of cultivated land was 89 km^2 over three years. According to the first and second national agricultural census data compilation, the acceleration of GDP has led to the construction of transportation infrastructure in the region, thus further accelerating the development of urban land and the loss of cultivated land resources. Besides, urban expansion is fierce in Jiangning District, Lishui District and Gaochun District, and rural urbanization accelerates the cultivated land decrease. For example, township enterprises in Nanjing are relatively developed, but their dispersed spatial distribution results in the non-agricultural transfer of a large number of cultivated land (Liu, Zhang, and Zhang 2013).Figure 7 shows that the net change in the area of cultivated land was large and sometimes small, but the trend of accelerated decrease did not change. In the past two decades, the net decrease in cultivated land has changed from 2 km^2 to 99 km^2 per year and the net decrease in the area has increased by dozens. The net change was the largest in 2007-2008, whereas the year of minimum net change was 1991-1992.

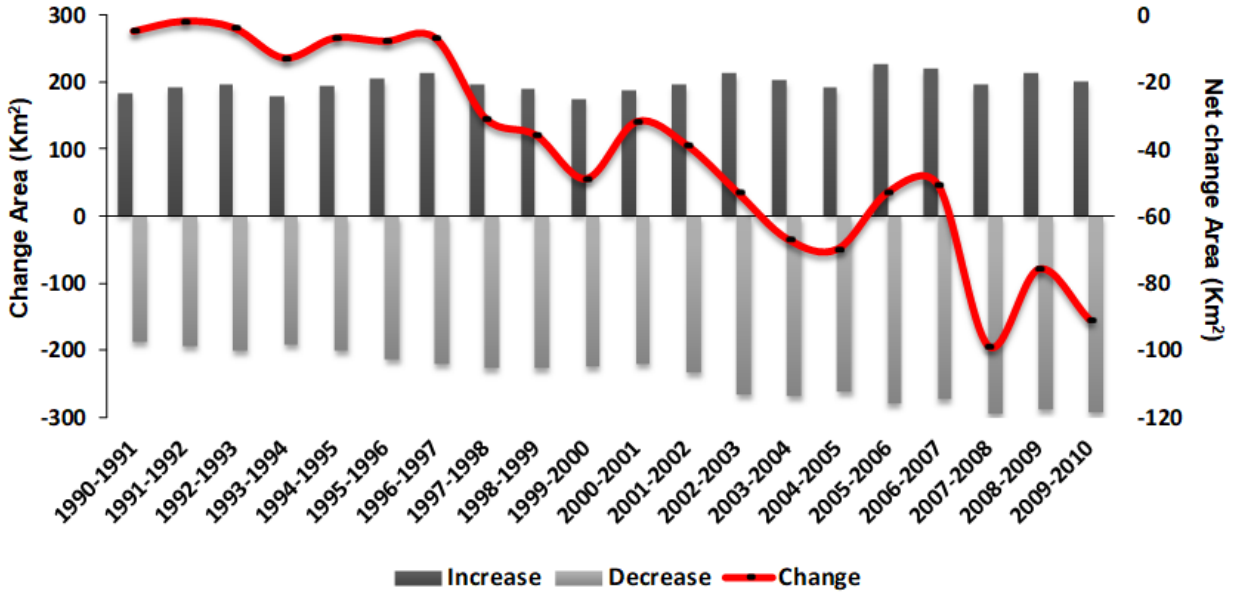

Figure 7. The annual change area of cultivated land from 1990 to 2010 in the study area.

4.3 Accuracy evaluation

Accuracy assessment of mapping of cultivated land dynamics is based on very high-resolution (VHR) image validation samples. To reasonably cover the validation samples, we collected the reference data from very high-resolution images from Google Earth and China's Land-Use/cover Datasets (CLUDs), which is a 30m resolution land use data from China. We selected 500 random sampling points per year from 1990 to 2010 as validation sample points, which corresponds to the spatial resolution of remotely sensed data, combined with VHR images and CLUDs data for classification sampling comparison. Stratified random sampling was used to obtain the validation sample to verify the accuracy of cultivated land dynamics.

The average overall mapping accuracy of the change in cultivated land dynamics map was 89.8%, with differences in the accuracy of four different types of cultivated land dynamics. Continuous

cultivated land and non-cultivated land had an average producer's and user's accuracies ranging from 89.9% to 92.3%. In contrast, with an average producer's and user's accuracy ranging from 87.6% to 88.9%, the accuracy of cultivated land increase and cultivated land decrease is relatively low (Table 2). Overall, the categories of cultivated land increase and cultivated land decrease show good accuracy in both producer's and user's accuracy with an average accuracy of over 87%.

Table 5. Overall, producer's and user's accuracies of annual cultivated land dynamics map.

Year	Producer's accuracy				User's accuracy				Overall accuracy
	Decrease	Increase	Continuous	Non	Decrease	Increase	Continuous	Non	
1990-1991	86.3	86.8	89.6	91.0	87.8	88.3	91.7	90.9	89.8
1991-1992	87.8	89.3	91.8	92.5	87.1	86.5	90.5	93.2	90.3
1992-1993	84.9	86.0	88.6	90.5	84.8	87.7	88.9	91.2	89.2
1993-1994	83.1	86.5	89.8	90.0	86.6	90.1	92.4	89.9	88.5
1994-1995	90.2	90.5	92.8	93.3	89.7	90.3	92.6	93.5	91.3
1995-1996	81.7	87.6	90.6	89.9	83.1	87.7	88.8	90.0	87.1
1996-1997	82.7	88.7	85.8	89.3	82.0	88.5	88.6	89.4	86.5
1997-1998	89.5	87.3	86.2	91.4	82.5	91.2	92.0	89.5	88.3
1998-1999	86.6	90.4	90.2	93.5	87.7	89.4	92.7	91.0	90.1
1999-2000	87.9	90.5	91.6	94.3	89.5	89.8	94.1	90.9	91.2
2000-2001	86.1	88.6	88.9	95.0	88.1	87.5	91.7	89.7	89.4
2001-2002	88.9	88.2	87.3	93.8	86.0	85.6	92.0	95.7	89.5
2002-2003	91.9	90.8	90.5	96.7	93.4	88.6	91.8	95.5	92.2
2003-2004	90.6	90.9	92.0	93.5	92.3	87.9	91.2	96.1	91.3
2004-2005	86.6	87.1	88.7	91.0	87.6	86.8	87.5	91.8	88.0
2005-2006	91.9	90.9	89.9	92.0	88.5	88.5	94.4	93.4	91.0
2006-2007	92.0	90.5	88.5	90.9	88.3	87.9	88.6	92.4	90.2
2007-2008	92.5	94.0	94.5	93.4	93.5	93.2	93.7	95.2	93.9
2008-2009	87.3	88.5	90.9	91.7	88.1	87.6	90.6	92.6	89.5
2009-2010	83.8	85.8	90.3	92.1	86.5	87.1	89.6	89.2	87.7
Mean	87.6	88.9	89.9	92.3	87.7	88.5	91.2	92.1	89.8

4.4 Assessment of cultivated land dynamics

In our study, we analyzed the spatial distribution of the frequency of change in cultivated land, because of the drastic changes in cultivated land cover types in the study area (Figure 8). Using the time series of cultivated land increase and decrease from 1990 to 2010, we calculated the frequency of cultivated land change per pixel by counting how often a pixel was identified as having increased in cultivated land or decreased in cultivated land for twenty years.

Overall, most of the cultivated land areas remained unchanged, accounting for 50.7% of the study area. Second, the change of cultivated land was less than two times in the past 20 years, accounting for 21.9% of our study area. Moreover, 16.4% of the total area was covered by 3 to 4 dynamic changes in cultivated land, and 8.3% of the total area was covered by 5 to 6 changes of cultivated land pixels, while only 2.7% of the total area was covered by more than 6 changes in cultivated land pixels.

Variable cultivated land in the study area mainly occurred around the mountains, hills, lakes and towns, and the frequency of change was mainly once. In contrast, the area of cultivated land farther away from the water and mountains generally did not change. The rapid expansion of cities and towns made the surrounding areas near cities change from cultivated land to residential land and the process of change was generally irreversible.

Through the spatial analysis of cultivated land dynamics in the study area, we show that the agricultural structure of Jiangpu District was changed from cultivated land to forest. Gaochun District and Dangtu County were sensitive areas for the change of cultivated land and water. These areas were close to lakes and dense river networks, resulting in large-scale transformation of cultivated land into crab ponds. The frequency of change was mostly 1 time, up to 3 times.

The areas where cultivated land changed twice were mainly located in the central part of Jiangpu District, and these areas were changed from forest to cultivated land and then to cities and towns. The drastic change of cultivated land occurred 3 to 4 times in the west of Shijiu Lake, and land cover classes changed frequently from the influence of inter-annual climate and human activities. Danggong polder were cultivated before 1995 and large areas of polders became water bodies due to floods in 1995. The remaining water bodies returned to cultivated land, except for several water bodies had turned into ponds by the end of 2000. Subsequently, more paddy fields turned into water with the expansion of aquaculture, resulting in the alternation of cultivated land and water bodies again. The area with 5 to 6 times or more dynamic changes of cultivated land were the most active areas in the study area, which were mainly distributed in the urban area of Nanjing, and were related to urban construction and urban greening.

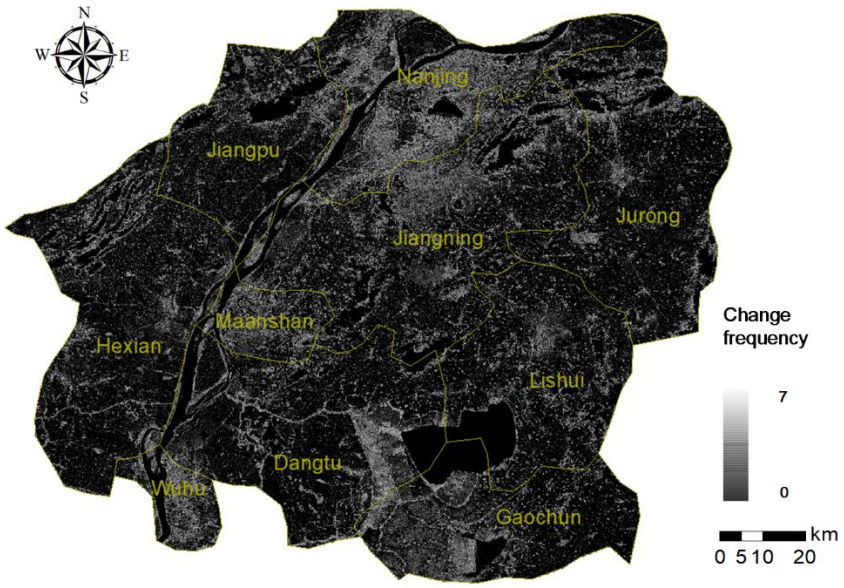

Figure 8. Frequency of cultivated land change from 1990 to 2010 in the study area

5. Discussion

Google Earth Engine (GEE) is a cloud computing platform specially designed to work with satellite images and other earth observation data, including not only the entire Landsat archive but also many other geophysical and environmental data (Patel et al. 2015). Compared with the traditional image processing tools, GEE can quickly process large amounts of remote sensing images, because it operates on Google cloud, which means its processing power is completely free from space and time constraints (Johansen, Phinn, and Taylor 2015). Therefore, the processing speed of mapping long time series cultivated land dynamics can be greatly accelerated, and users are almost entirely unaffected by the working details of the parallel processing environment, because Google Earth Engine hides almost all the specific calculations.

In the meantime, the cultivated land can be better classified from land cover data by inter-annual NDVI calculated from long-term remote sensing images, and GEE also provides a rudimentary cloud scoring algorithm for scoring Landsat pixels to reduce the impact of clouds and cloud shadows. The GEE is also designed to make it easier for researchers to publish their results for other researchers and decision makers, and even for the public. Once researchers develop algorithms on the Earth Engine, the system's data products or interactive applications can be generated on the GEE cloud computing platform, therefore, researchers do not need to develop applications or network programming.

The feasibility of using NDVI trajectory to detect dynamic change of cultivated land in long time series is also studied in this paper. A simple and efficient algorithm can be generated by combining inter-annual NDVI time series with the available image data in each year based on Google Earth Engine. In addition, the problem of corresponding coarse-resolution of NDVI trajectories in high temporal resolution remote sensing images is solved by using the spatiotemporal fusion model (ESTARFM). Compared with the coarse-resolution MODIS NDVI used in previous studies, the fine-resolution synthetic Landsat NDVI time series plays an important role in the study of fine-scale cultivated land dynamic change. In addition, we can better distinguish cultivated land with other types of vegetation by using the phenological characteristics of the NDVI trajectory, which is needed to understand the phenological characteristics in the study area. In the meantime, we will consider comparing different vegetation indices in the future (Atkinson et al. 2012).

6. Conclusions

The objective of this study is to evaluate a way of mapping a detailed spatial distribution of cultivated land annual dynamics in a high spatiotemporal resolution in Middle-lower Yangtze Plain based on GEE. The annual dynamics of cultivated land in Middle-lower Yangtze Plain were first produced at 30 m resolution with a one-year interval in 1990-2010.We first extracted the increase or decrease in vegetation using the breakpoints and time periods of time series the inter-annual NDVI trajectory. Next, we used the ESTRAFM algorithm to generate a synthetic NDVI with high spatial and temporal resolution, which was used as the database for detecting the cultivated land dynamics. Importantly, based on synthetic high spatial-temporal resolution Landsat NDVI time-series data, we separated cultivated land dynamics from non-cultivated land dynamics by detecting phenological characteristic,

and successfully mapped annual long time-series cultivated land change in Middle-lower Yangtze Plain from 1990 to 2010. The assessment of cultivated land dynamic mapping confirmed the reliability of our method, which can be used to quickly and accurately map continuous long-term changes in agricultural land.

Our results finally show that the total area of cultivated land in the Middle-lower Yangtze Plain has been decreasing from 1990 to 2010. In addition, we found that the cultivated land total area had decreased, because the area of decrease in cultivated land was always more than the area on increase. The rate of reduction in the area of cultivated land in the two decades has become faster and the decrease of cultivated land has become more intense since 1997. The change in cultivated land in the study area mainly occurred in the mountains, hills, lakes and around towns, and the change frequency of these area was mainly one or two times. The region with more dynamic changes in cultivated land mainly distributes in Nanjing urban area, which is closely related to urban greening and infrastructure construction. Future work will focus on extending the method of detecting cultivated land dynamics by long time-series trajectory methods to the national level.

Acknowledgement

This research was supported by the National Key R&D Program of China (Grant No. 2017YFA0604401, 2017YFA0604402 and 2017YFA0604404), the National Natural Science Foundation of China (Grant No. 41601420). The authors are grateful to Xinchang Zhang, Ziyu Lin, who had assisted or advised them during various stages of this work

References

Atkinson, Peter M., C. Jeganathan, Jadu Dash, and Clement Atzberger. 2012. "Inter-comparison of four models for smoothing satellite sensor time-series data to estimate vegetation phenology." *Remote Sensing of Environment* 123:400-17. doi: https://doi.org/10.1016/j.rse.2012.04.001.

Basnet, Bikash, and Anthony Vodacek. 2015. "Tracking land use/land cover dynamics in cloud prone areas using moderate resolution satellite data: A case study in Central Africa." *Remote Sensing* 7 (6):6683-709.

Beurs, K. M. de, G. M. Henebry, and A. A. Gitelson. 2004. Regional MODIS analysis of abandoned agricultural lands in the Kazakh steppes. Paper presented at the IGARSS 2004. 2004 IEEE International Geoscience and Remote Sensing Symposium, 20-24 Sept. 2004.

Camilo, Alcantara, Kuemmerle Tobias, Baumann Matthias, V. Bragina Eugenia, Griffiths Patrick, Hostert Patrick, Knorn Jan, et al. 2013. "Mapping the extent of abandoned farmland in Central and Eastern Europe using MODIS time series satellite data." *Environmental Research Letters* 8 (3):035035.

Estel, Stephan, Tobias Kuemmerle, Camilo Alcántara, Christian Levers, Alexander Prishchepov, and Patrick Hostert. 2015. "Mapping farmland abandonment and recultivation across Europe using MODIS NDVI time series." *Remote Sensing of Environment* 163:312-25. doi: https://doi.org/10.1016/j.rse.2015.03.028.

Feng, Gao, J. Masek, M. Schwaller, and F. Hall. 2006. "On the blending of the Landsat and MODIS surface reflectance:

predicting daily Landsat surface reflectance." *IEEE Transactions on Geoscience and Remote Sensing* 44 (8):2207-18. doi: 10.1109/TGRS.2006.872081.

Foley, Jonathan A., Navin Ramankutty, Kate A. Brauman, Emily S. Cassidy, James S. Gerber, Matt Johnston, Nathaniel D. Mueller, et al. 2011. "Solutions for a cultivated planet." *Nature* 478:337. doi: 10.1038/nature10452 https://www.nature.com/articles/nature10452#supplementary-information.

Gong, Peng, Jie Wang, Le Yu, Yongchao Zhao, Yuanyuan Zhao, Lu Liang, Zhenguo Niu, et al. 2013. "Finer resolution observation and monitoring of global land cover: first mapping results with Landsat TM and ETM+ data." *International Journal of Remote Sensing* 34 (7):2607-54. doi: 10.1080/01431161.2012.748992.

Gorelick, Noel, Matt Hancher, Mike Dixon, Simon Ilyushchenko, David Thau, and Rebecca Moore. 2017. "Google Earth Engine: Planetary-scale geospatial analysis for everyone." *Remote Sensing of Environment* 202:18-27. doi: https://doi.org/10.1016/j.rse.2017.06.031.

Graesser, Jordan, Navin Ramankutty, T. Mitchell Aide, and H. Ricardo Grau. 2015. "Cropland/pastureland dynamics and the slowdown of deforestation in Latin America." *Environmental Research Letters* 10 (3):10. doi: DOI:101088/1748-9326/10/3/034017.

Guo, D. 2014. "China Statistical Yearbook for Regional Economy." In.: China Statistics Press, Beijing.

Hilker, Thomas, Michael A. Wulder, Nicholas C. Coops, Nicole Seitz, Joanne C. White, Feng Gao, Jeffrey G. Masek, and Gordon Stenhouse. 2009. "Generation of dense time series synthetic Landsat data through data blending with MODIS using a spatial and temporal adaptive reflectance fusion model." *Remote Sensing of Environment* 113 (9):1988-99. doi: https://doi.org/10.1016/j.rse.2009.05.011.

Huang, Huabing, Yanlei Chen, Nicholas Clinton, Jie Wang, Xiaoyi Wang, Caixia Liu, Peng Gong, Jun Yang, Yuqi Bai, and Yaomin Zheng. 2017. "Mapping major land cover dynamics in Beijing using all Landsat images in Google Earth Engine." *Remote Sensing of Environment* 202:166-76.

Jamali, Sadegh, Jonathan Seaquist, Lars Eklundh, and Jonas Ardö. 2014. "Automated mapping of vegetation trends with polynomials using NDVI imagery over the Sahel." *Remote Sensing of Environment* 141:79-89.

Jin, Yuhao, Xiaoping Liu, Yimin Chen, and Xun Liang. 2018. "Land-cover mapping using Random Forest classification and incorporating NDVI time-series and texture: a case study of central Shandong." *International Journal of Remote Sensing*:1-21. doi: 10.1080/01431161.2018.1490976.

Johansen, Kasper, Stuart Phinn, and Martin Taylor. 2015. "Mapping woody vegetation clearing in Queensland, Australia from Landsat imagery using the Google Earth Engine." *Remote Sensing Applications: Society and Environment* 1:36-49. doi: https://doi.org/10.1016/j.rsase.2015.06.002.

Liang, Xun, Xiaoping Liu, Xia Li, Yimin Chen, He Tian, and Yao Yao. 2018. "Delineating multi-scenario urban growth boundaries with a CA-based FLUS model and morphological method." *Landscape and Urban Planning* 177:47-63. doi: https://doi.org/10.1016/j.landurbplan.2018.04.016.

Liu, Jiyuan, Wenhui Kuang, Zengxiang Zhang, Xinliang Xu, Yuanwei Qin, Jia Ning, Wancun Zhou, Shuwen Zhang, Rendong Li, and Changzhen Yan. 2014. "Spatiotemporal characteristics, patterns, and causes of land-use changes in China since the late 1980s." *Journal of Geographical Sciences* 24 (2):195-210.

Liu, Jiyuan, Wenhui Kuang, Zengxiang Zhang, Xinliang Xu, Yuanwei Qin, Jia Ning, Wancun Zhou, et al. 2014. "Spatiotemporal characteristics, patterns, and causes of land-use changes in China since the late 1980s." *Journal of Geographical Sciences* 24 (2):195-210. doi: 10.1007/s11442-014-1082-6.

Liu, Xiaoping, Guohua Hu, Yimin Chen, Xia Li, Xiaocong Xu, Shaoying Li, Fengsong Pei, and Shaojian Wang. 2018. "High-resolution multi-temporal mapping of global urban land using Landsat images based on the Google Earth Engine Platform." *Remote Sensing of Environment* 209:227-39. doi: https://doi.org/10.1016/j.rse.2018.02.055.

Liu, Xiaoping, Xun Liang, Xia Li, Xiaocong Xu, Jinpei Ou, Yimin Chen, Shaoying Li, Shaojian Wang, and Fengsong Pei. 2017. "A future land use simulation model (FLUS) for simulating multiple land use scenarios by coupling human and

natural effects." *Landscape and Urban Planning* 168:94-116. doi: https://doi.org/10.1016/j.landurbplan.2017.09.019.

Patel, Nirav N., Emanuele Angiuli, Paolo Gamba, Andrea Gaughan, Gianni Lisini, Forrest R. Stevens, Andrew J. Tatem, and Giovanna Trianni. 2015. "Multitemporal settlement and population mapping from Landsat using Google Earth Engine." *International Journal of Applied Earth Observation and Geoinformation* 35:199-208. doi: https://doi.org/10.1016/j.jag.2014.09.005.

Savitzky, Abraham, and Marcel Golay. 1964. "Smoothing and Differentiation of Data by Simplified Least Squares Procedures." *Analytical Chemistry* 36 (8):1627. doi: citeulike-article-id:5416908.

Schmidt, Michael, Richard Lucas, Peter Bunting, Jan Verbesselt, and John Armston. 2015. "Multi-resolution time series imagery for forest disturbance and regrowth monitoring in Queensland, Australia." *Remote Sensing of Environment* 158:156-68. doi: https://doi.org/10.1016/j.rse.2014.11.015.

Wardlow, Brian D., and Stephen L. Egbert. 2008. "Large-area crop mapping using time-series MODIS 250 m NDVI data: An assessment for the U.S. Central Great Plains." *Remote Sensing of Environment* 112 (3):1096-116. doi: https://doi.org/10.1016/j.rse.2007.07.019.

White, Michael A., Peter E. Thornton, and Steven W. Running. 1997. "A continental phenology model for monitoring vegetation responses to interannual climatic variability." *Global biogeochemical cycles* 11 (2):217-34.

Xiong, Jun, S. Prasad Thenkabail, C. James Tilton, K. Murali Gumma, Pardhasaradhi Teluguntla, Adam Oliphant, G. Russell Congalton, Kamini Yadav, and Noel Gorelick. 2017. "Nominal 30-m Cropland Extent Map of Continental Africa by Integrating Pixel-Based and Object-Based Algorithms Using Sentinel-2 and Landsat-8 Data on Google Earth Engine." *Remote Sensing* 9 (10). doi: 10.3390/rs9101065.

Yu, Le, and Peng Gong. 2012. "Google Earth as a virtual globe tool for Earth science applications at the global scale: progress and perspectives." *International Journal of Remote Sensing* 33 (12):3966-86. doi: 10.1080/01431161.2011.636081.

Yu, Le, Jie Wang, Nicholas Clinton, Qinchuan Xin, Liheng Zhong, Yanlei Chen, and Peng Gong. 2013. "FROM-GC: 30 m global cropland extent derived through multisource data integration." *International Journal of Digital Earth* 6 (6):521-33. doi: 10.1080/17538947.2013.822574.

Zhu, Xiaolin, Jin Chen, Feng Gao, Xuehong Chen, and Jeffrey G. Masek. 2010. "An enhanced spatial and temporal adaptive reflectance fusion model for complex heterogeneous regions." *Remote Sensing of Environment* 114 (11):2610-23. doi: https://doi.org/10.1016/j.rse.2010.05.032.